University of Nebraska - Lincoln
DigitalCommons@University of Nebraska - Lincoln

US Department of Energy Publications | US Department of Energy

1-1-2001

Kinetic Analysis of the Bacterial Reduction of Goethite

Chongxuan Liu
Pacific Northwest National Laboratory, chongxuan.liu@pnl.gov

John M. Zachara
Pacific Northwest National Laboratory, john.zachara@pnl.gov

James K. Fredrickson
Pacific Northwest National Laboratory, jim.fredrickson@pnl.gov

Cynthia Brinkman
Pacific Northwest National Laboratory

Follow this and additional works at: http://digitalcommons.unl.edu/usdoepub

Part of the Bioresource and Agricultural Engineering Commons

Liu, Chongxuan; Zachara, John M.; Fredrickson, James K.; and Brinkman, Cynthia, "Kinetic Analysis of the Bacterial Reduction of Goethite" (2001). *US Department of Energy Publications.* Paper 218.
http://digitalcommons.unl.edu/usdoepub/218

This Article is brought to you for free and open access by the US Department of Energy at DigitalCommons@University of Nebraska - Lincoln. It has been accepted for inclusion in US Department of Energy Publications by an authorized administrator of DigitalCommons@University of Nebraska - Lincoln.

Environ. Sci. Technol. **2001**, *35,* 2482−2490

Kinetic Analysis of the Bacterial Reduction of Goethite

CHONGXUAN LIU,* SREENIVAS KOTA, JOHN M. ZACHARA, JIM K. FREDRICKSON, AND CYNTHIA K. BRINKMAN

Pacific Northwest National Laboratory, P.O. Box 999, MS K8-96, Richland, Washington 99352

The kinetics of dissimilatory reduction of goethite (α-FeOOH) was studied in batch cultures of a groundwater bacterium, *Shewanella putrefaciens,* strain CN32 in pH 7 bicarbonate buffer. The rate and extent of goethite reduction were measured as a function of electron acceptor (goethite) and donor (lactate) concentrations. Increasing goethite concentrations increased both the rate and extent of Fe(III) reduction when cell and lactate concentrations were held constant. However, constant initial reduction rates were observed after normalization to the Fe(II) sorption capacity of FeOOH, suggesting that the bacterial reduction rate was first order with respect to surface site concentration. Increasing the lactate concentration also increased the rate and extent of FeOOH reduction. Monod-type kinetic behavior was observed with respect to lactate concentration. Fe(II) sorption on FeOOH was well-described by the Langmuir sorption isotherm. However, the Fe(II) sorption capacities hyperbolically decreased with increasing FeOOH concentration (10−100 mM) implying aggregation, while the affinity constant between Fe(II) and goethite was constant (log $K \approx 3$). Evaluation of the end states of the variable FeOOH and lactate experiments when iron reduction ceased indicated a consistent excess in reaction free energy of −22.7 kJ/mol. This value was remarkably close to the minimum value reported for bacteria to mediate a given reaction (−20 kJ/mol). X-ray diffraction (XRD) and scanning electron microscopy (SEM) indicated that siderite ($FeCO_3$) was the only biogenic Fe(II) solid formed upon FeOOH bioreduction. A kinetic biogeochemical model that incorporated Monod kinetics with respect to lactate concentration, first-order kinetics with respect to goethite surface concentration, a Gibbs free energy availability factor, the rates of Fe(II) sorption on goethite and siderite precipitation, and aqueous speciation reactions was applied to the experimental data. Using independently estimated parameters, the developed model successfully described bacterial goethite reduction with variable FeOOH and lactate concentrations.

Introduction

Dissimilatory microbial reduction of Fe(III) oxides is an important process in the iron biogeochemical cycle that influences iron diagenesis and mineralization in anoxic environments. The rate and extent of Fe(III) oxide reduction by DIRB are influenced by a variety of interrelated factors including: organism/oxide contact *(1−3)*; the crystallinity, particle size/surface area, and phase identity of the Fe(III) oxides *(1, 4−9)*; sorption of Fe(II) on the residual Fe(III) oxide *(10−14)* and/or the cell surface *(13, 15)*; Fe(II) biomineralization *(11, 12)*; quinone-containing humic substances *(11, 12, 16, 17)* that mediate electron transfer between bacterial cell and oxide surfaces; and organic ligands that enhance Fe(III) dissolution or Fe(II) solubilization *(6, 18)*. Quantitative interrelationships between these factors and rate expressions regarding the DIRB mediated reductive dissolution of Fe(III) oxides, however, have not been established.

The kinetics of bacterial degradation of organic compounds and transfer of electrons to acceptors generally follows the Monod rate expression. Monod kinetics have been widely applied in biogeochemical reactive transport models *(19−30)*. However, the applicability of Monod kinetics for dissimilatory Fe(III) reduction has not been critically examined. The Monod rate expression with respect to the electron acceptor was found to describe the microbial reduction of complexed aqueous Fe(III) *(15)*, but applications to solid-phase Fe(III) oxides have not been reported. One investigation suggested that the bioreduction of hematite followed saturation type kinetics (Monod) *(1)*, but more recent studies using higher concentrations of iron oxides (e.g., 50 mM of hydrous ferric oxide (HFO), goethite, and hematite *(9−12)*) support more complex kinetic scenarios. A key issue associated with the application of the Monod model to bacterial Fe(III) oxide reduction is how to define the electron acceptor concentration (e.g., that of the Fe(III) oxide) and its temporal dynamics during bioreduction. Biogeochemical reactions (e.g., adsorption, precipitation, and dissolution) that may influence the effective concentration or mole-balance of the electron acceptor (e.g. the Fe(III) oxide) and biogenic Fe(II) are important considerations.

The crystalline Fe(III) oxide/DIRB system represents an interesting test case for the applicability of Monod kinetics to a solid-phase electron acceptor because the bioreduction of goethite and hematite *(9, 11)* ceases earlier than a simple saturation model (Monod) would predict. Almost all batch bioreduction studies with crystalline Fe(III) oxides have shown that only a limited fraction of the solid phase can be reduced even with excess electron donor *(9−13, 18)*. Reaction suppression by biogenic Fe(II) and thermodynamic intractability are two potential causes of this behavior, as are physiologic explanations. Biogenic Fe(II) may adsorb to or precipitate on the residual oxide and DIRB surface *(11−13, 15)*. Such reactions may mask or consume surface sites (on the electron acceptor) and interfere with electron transfer between membrane bound proteins and the oxide surface. The kinetic behavior of crystalline Fe(III) oxide bioreduction may also be regulated by thermodynamics. The overall reaction free energy of reductive dissolution of goethite decreases as reaction products accumulate and reactants consume. When a solution thermodynamically approaches to saturation state (equilibrium), the dissolution rate of goethite decreases and approaches to zero *(31)*.

In this communication we evaluate the applicability of the Monod kinetic model to the bioreduction of goethite by a groundwater DIRB (*Shewanella putrefaciens* strain CN32). Batch experiments were performed where the concentrations of both electron donor (lactate) and electron acceptor (goethite) were varied in an attempt to parametrize a saturation-type kinetic model. Aqueous and sorbed concentrations of biogenic Fe(II) were monitored with time, and solid-phase Fe(II) biomineralization products were deter-

* Corresponding author phone: (509)376-0129; fax: (509)376-3650; e-mail: chongxuan.liu@pnl.gov.

10.1021/es001956c CCC: $20.00 © 2001 American Chemical Society
Published on Web 05/04/2001

This article is a U.S. government work, and is not subject to copyright in the United States.

mined at experiment termination. Interaction experiments of $Fe(II)_{(aq)}$ with goethite and CN32 were performed independently to parametrize Fe(II) sorption reactions on their surfaces. It was concluded that a simple Monod-type model could not describe the bioreduction data. However the experimental system could be well described by incorporating (1) material balance and kinetic effects of Fe(II) sorption and $FeCO_3$ precipitation on FeOOH surface site availability and (2) a thermodynamic factor to account for available free energy of reaction above that required for intracellular adenosine triphosphate (ATP) synthesis. Neither of these additions to the Monod model, alone, could account for the complex temporal dynamics of FeOOH bioreduction.

Experimental Procedures

Materials. Goethite (α-FeOOH; 60.2 m^2/g) was prepared by hydrolysis of $FeCl_3 \bullet 6H_2O$ solution and aging at elevated temperatures (70 °C) according to procedures of Schwertmann and Cornell *(32)*. Following preparation, the goethite was dialyzed against deionized, distilled H_2O to remove soluble salts. The dialyzed goethite was stored in suspension at 4 °C to minimize aggregation that may accompany drying. The goethite suspension was sonicated prior to experimentation in order to maximize the dispersion of FeOOH particles.

Shewanella putrefaciens (strain CN32) is a DIRB that was isolated from an anaerobic aquifer in northwestern New Mexico *(33)*. The details of culturing procedures and CN32 cell harvest have been described elsewhere *(11, 12)*. For the FeOOH reduction experiments, harvested CN32 cells were resuspended in a defined medium buffered with bicarbonate. The composition of the medium was (mM) NH_4Cl (28.0), Na_2HPO_4 (0.44), KCl (1.20), $CaCl_2 \bullet 2H_2O$ (0.61), and $NaHCO_3$ (30.0). The medium was supplemented with 10 mL each of vitamin and trace mineral solutions described previously *(34)*. L-Lactic acid (ICN biochemicals) at various concentrations (0.5−30 mM) served as the electron donor. The medium was dispensed into 60 mL serum bottles purged with O_2-free N_2:CO_2 (80:20), stoppered with butyl rubber closures, and crimp sealed.

Sorption Measurements. The sorption of Fe(II) by FeOOH was measured under anaerobic conditions in glass pressure tubes as a function of Fe(II) (0−10 mM) and FeOOH concentration (10−100 mM). PIPES (1,4-piperazinediethanesulfonic acid) buffer was used instead of bicarbonate buffer to avoid siderite precipitation. All samples were allowed to equilibrate for 1 h under continuous mixing (100 rpm). Kinetic measurements indicated that Fe(II) sorption reached equilibrium in less than 30 min. After equilibration, the suspensions were filtered (0.2 μm or 1.8 nm) and acidified (1 N HCl). Fe(II) in the acidified filtrates was measured using the ferrozine assay. Sorbed Fe(II) was calculated from the difference between the total and final aqueous Fe(II) concentrations.

Kinetic Assay. CN32 cells (2×10^8 cells/mL) were mixed with variable concentrations of FeOOH [5(0.44), 10(0.89), and 100(8.9) mM (g/L)] and lactate (0.5, 2, 10, and 20 mM) in 50 mL of media and incubated anaerobically at 25 °C with continuous shaking (100 rpm). Replicate suspension subsamples (1 mL) were removed at selected time-points using a sterile needle and syringe. The samples were separated into two aliquots: 0.5 mL was filtered through 0.2 μm polycarbonate filter directly to 0.5 mL of 0.5 N HCl and another was directly added to 0.5 mL of 1N HCl. Both samples were analyzed by ferrozine assay for Fe(II). The filtered fraction is reported herein as aqueous Fe(II) and the unfiltered fraction as total Fe(II).

X-ray Diffraction and Electron Microscopy. Mineral residues from the reduction experiments were mixed with glycerol under anaerobic conditions, and the solid slurry was smeared on a glass slide for X-ray diffraction (XRD) analyses. The slides were maintained under anoxic conditions until the time of analysis. The X-ray source was a Phillips XRG31000 X-ray generator operating a fixed-anode, long-fine-focus Cu tube at 45 Kv, 40 mA (1800 W). The International Center for Diffraction Data, Powder Diffraction File database on CD-ROM (ICD PDF-2, Sets 1−46 1996) was the source of reference diffraction data. Glycerol contributed an X-ray diffraction peak that was removed from the diffractogram by background subtraction. Untreated, bioreduced mineral residues were also dried under anoxic conditions and were examined using a field emission scanning electron microscope (FESEM) (LEO, 982) at 5 ke V and 90 uA to obtain crystal morphology *(11)*.

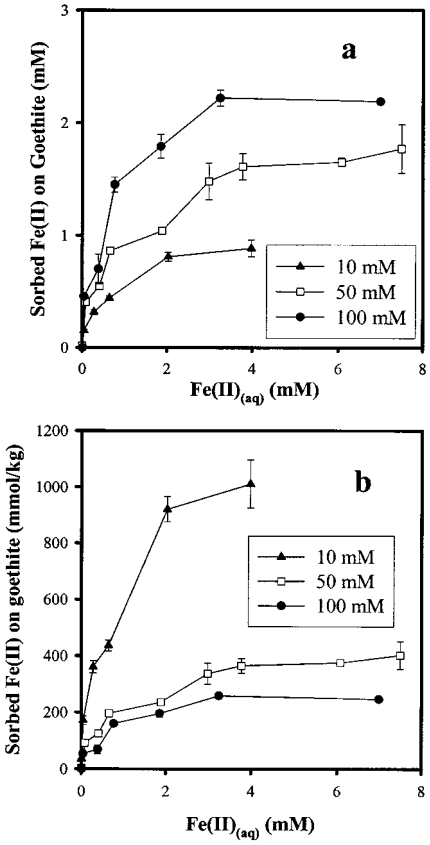

FIGURE 1. The sorption of Fe(II) in goethite suspensions of different densities: (a) total concentration isotherm and (b) mass normalized isotherm.

Experimental Results

Sorption of Fe(II) with Variable Goethite Concentration. The total amount of Fe(II) sorbed to FeOOH increased with increasing solids concentration (Figure 1a). However, the Fe(II) adsorption density [mmol Fe(II)/kg] decreased with increasing goethite concentration (Figure 1b). The maximum sorption density was over 1 mol Fe(II)/kg for 10 mM FeOOH, decreasing to approximately 250 mmol Fe(II)/kg for 100 mM FeOOH. The decrease in sorption density was consistent with particle aggregation that blocked Fe(II) sorption sites at higher solid concentrations. Visual observations indicated that the FeOOH particles were increasingly aggregated at higher solid concentrations. Particle aggregation is significant in that bacterial reduction is believed to require direct contact with the oxide surface, and aggregation may decrease the effective surface area of the Fe(III) oxide accessible for contact with the organism surface.

Initial Goethite Reduction Rates. The initial FeOOH reduction rate increased with increasing FeOOH and lactate concentration (Figure 2). The rate increased from 0.02 mM/h

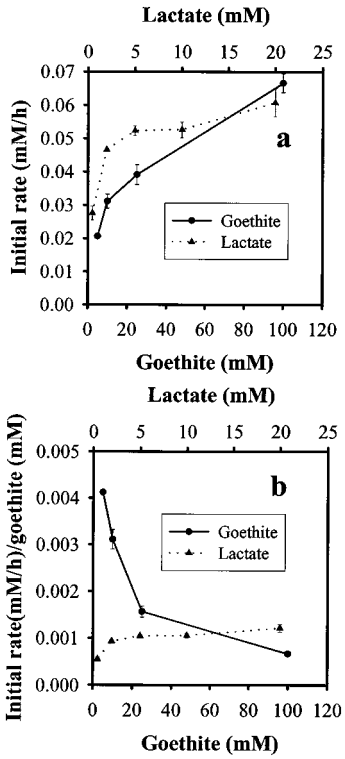

FIGURE 2. Goethite reduction rates as a function of lactate concentration and suspension density (a fixed 30 mM lactate for variable FeOOH cases and a fixed 50 mM FeOOH for variable lactate cases; all cases with 30 mM bicarbonate): (a) overall bioreduction rates and (b) mass normalized reduction rates.

at 5 mM FeOOH to 0.065 mM/h at 100 mM FeOOH (Figure 2a). However, the reduction rate decreased with increasing FeOOH concentration when the rate was normalized to goethite concentration (Figure 2b). This effect could be due to saturation-type kinetics with respect to goethite *(35, 36)* or to a decrease in available surface area per unit goethite mass with increasing goethite concentration as suggested by the sorption experiments (Figure 1). The changes in the initial reduction rate with the lactate concentration were typical of Monod type kinetics (Figure 2a,b), i.e., the reduction rate increased rapidly with increasing lactate concentration from 0.5 to 5 mM and then saturated at higher electron donor concentrations.

Goethite Reduction with Variable Goethite and Lactate Concentrations. The rate and extent of FeOOH reduction increased with increasing FeOOH concentration when lactate was held constant (Figure 3). However, the percentage of goethite reduction decreased with increasing solid concentration, 64% at 5 mM, 50% at 10 mM, and 10% at 100 mM. In all cases, FeOOH was only partially reduced, similar to previous reports using 50 mM goethite with *S. putrefaciens* (CN32) *(11)* and *Shewanella alga* (BrY) *(9, 10, 13)*. The electron donor, lactate (30 mM), was in excess of that required to reduce all of the Fe(III) to Fe(II) assuming a 4:1 stoichiometry of Fe(II) production to lactate oxidation (to CO_2 and acetate). The lactate consumption at experiment termination was less than 3 mM in all the variable goethite treatments. The difference between total and aqueous Fe(II) increased with goethite concentration (Figure 3), suggesting that more biogenic Fe(II) was adsorbed or precipitated at higher goethite concentration. Such behavior was an anticipated consequence of the variable FeOOH site concentration.

The rate and extent of FeOOH reduction also increased with increasing lactate concentration (Figure 4), although the reduction of goethite at higher lactate concentrations

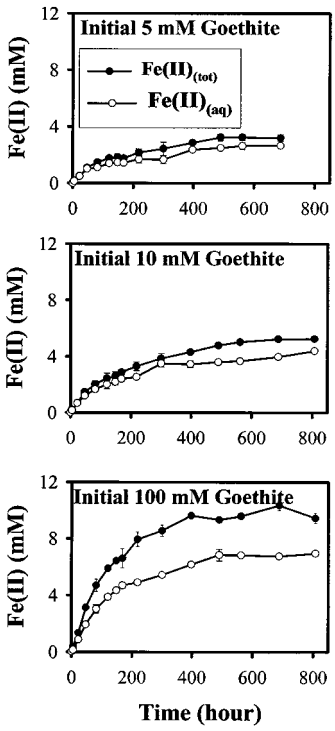

FIGURE 3. Fe(II) production (total and aqueous) in goethite suspensions of different densities [lactate = 30 mM and bicarbonate = 30 mM].

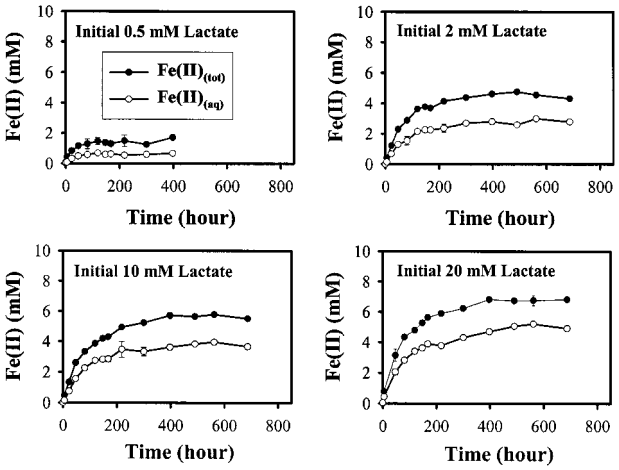

FIGURE 4. Fe(II) production (total and aqueous) in goethite suspensions with variable initial lactate concentrations [goethite = 50 mM and bicarbonate = 30 mM].

ceased considerably earlier than a saturation model would predict. The percentages of goethite reduction were 3.4, 8.6, 11, and 14% (a saturation model predicts 4, 16, 80, 100%) at 0.5, 2, 10, 20 mM lactate concentrations, respectively.

Solid Analysis. Siderite was the only observed secondary mineral product resulting from the bioreduction of goethite (Figure 5) as indicated by a predominant *d* spacing of 0.28 nm at 32° 2θ. The presence of siderite ($FeCO_3$) was confirmed by SEM (Figure 6); $FeCO_3$ formed both in association with FeOOH and as discrete 0.25−0.50 μm rhombohedral precipitates. Vivianite was not observed by XRD or SEM despite the presence of PO_4^{3-} in the medium (0.44 mM).

Analysis and Discussion

Fe(II) Sorption. Fe(II) sorption on FeOOH followed the Langmuir isotherm (Figure 7a). However, the sorption capacity (Q_{max}) decreased with increasing goethite concen-

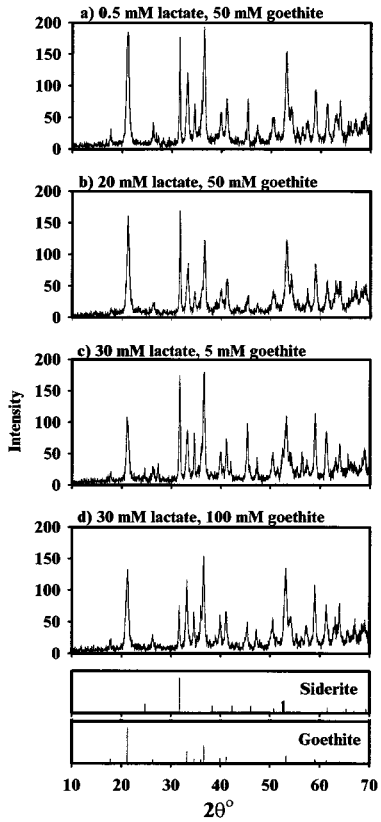

FIGURE 5. X-ray diffractograms of residual solids at the end of goethite bioreduction experiments. Results are shown for variable lactate and variable goethite experiments (goethite and siderite are the crystalline phases present).

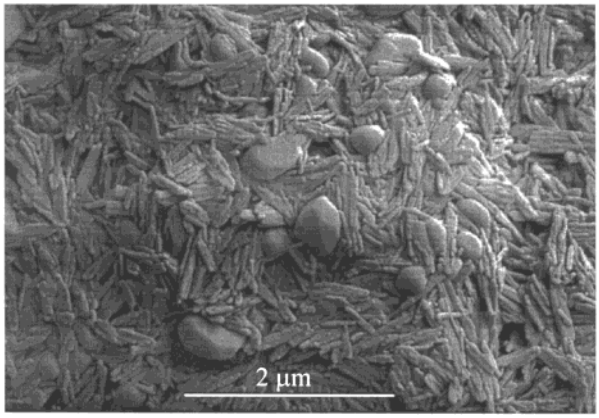

FIGURE 6. Scanning electron micrograph of residual solids after goethite bioreduction. Siderite ($FeCO_3$) is present as pseudorhomdohedral precipitates ranging from 0.25 to 0.5 μm in size.

tration from 10 to 100 mM, while the affinity constant between Fe(II) and goethite remained constant (log $K = 3-3.1$). The variation in sorption capacity with particle concentration has been referred to as the particle concentration effect (PCE). The PCE has been observed in natural waters, such as in estuaries *(37−39)*, rivers *(40)*, and lakes *(41)*, and in laboratory experiments with natural and synthetic particles *(42−44)*. It has been attributed to either incomplete filtration of colloids *(37, 40, 45, 46)* or particle aggregation *(38, 47−49)*. A PCE due to incomplete filtration was discounted here by comparing Fe(II) concentrations in 0.2 μm and 1.8 nm filtrates. These were found to be virtually identical (with random relative errors of 0−4.5%). Therefore, particle aggregation appeared as the most plausible explanation for the change of sorption capacity with goethite concentration.

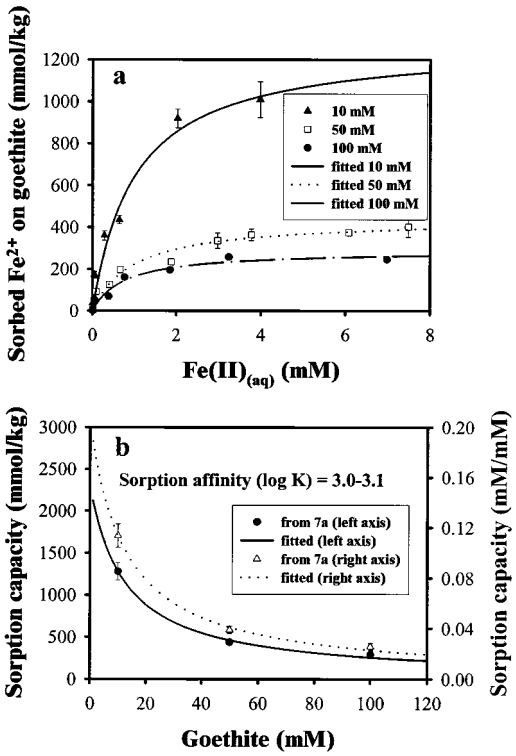

FIGURE 7. (a) Fe(II) sorption data on goethite fitted to the Langmuir isotherm and (b) the fitted Langmuir sorption capacities (from part a) change with goethite concentration and follow a hyperbolic function.

The sorption capacities of goethite hyperbolically decreased with increasing goethite concentration (Figure 7b):

$$Q_{max}(C_{goethite})\ (\mathrm{mM/mM}) = 2.57(12.6 + C_{goethite})^{-1} \quad (C_{geothite}\ \text{in mM}) \quad (1)$$

Using the sorption capacity, Q_{max}, calculated from eq 1, the sorption isotherm for a specific FeOOH concentration could be expressed as

$$q(\mathrm{mM}) = Q_{max}C_{Fe(II)}(b + C_{Fe(II)})^{-1} \quad (2)$$

where b is the inverse of the affinity coefficient, K (log $K = 3.0-3.1$), and q is the adsorbed concentration.

Reduction Rate with Respect to Electron Donor and Acceptor Concentrations. Previous studies *(9)* have normalized the reduction rate to surface area because of the apparent contact requirement between the DIRB and the Fe(III) oxide surface *(6, 50)*. Defining the surface area concentration (m^2/L) of an Fe(III) oxide suspension can be problematic. The drying of fine-grained Fe(III) oxides as required for powder gas adsorption measurement (BET) of surface area induces particle aggregation that may be difficult to reverse on resuspension and that may affect organism/oxide interfacial contact. In-situ methods exist for the surface area of charged particles (e.g., negative adsorption *(51)*), but these require assumptions about particle shape and site density that may not be easily justified. Here, we normalized the initial reduction rates (Figure 8) to the sorption capacity of FeOOH for Fe(II). Fe(II) sorption capacity was used as a surrogate parameter for surface area because it is proportional to the active surface area of the Fe(III) oxide *(52, 53)*, can be readily measured in the media of interest, and is linked to material balance relationships of the key system chemical components (Table 1). Nevertheless, it is important to recognize that the rate parameters used in the following analysis are referenced

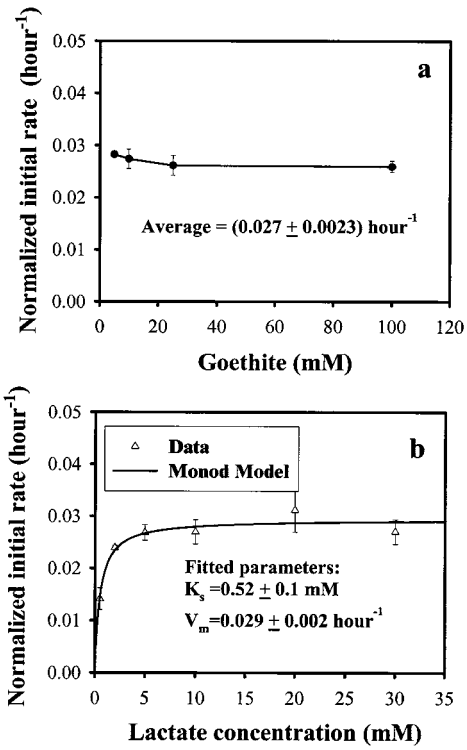

FIGURE 8. (a) The initial rates of bacterial goethite reduction (with 30 mM lactate) normalized by the goethite sorption capacity for Fe(II) (the line is merely connecting data). (b) The normalized initial rates follow Monod type kinetics with respect to lactate concentration. The estimated Monod parameters were 0.029 h^{-1} for the maximum reduction rate (V_m) and 0.52 mM for the half-saturation constant.

to the Fe(II) sorption capacity that is used as a surrogate measure of the electron acceptor concentration. Sorption capacity in a microbe-inoculated suspension can be affected by minor changes in experimental variables and may differ from comparable abiotic systems *(*e.g., ref *54)* as a result of microbe-induced flocculation.

The normalized reduction rates at variable FeOOH concentrations were relatively constant at 0.027 (±0.0023) h^{-1} (Figure 8a), indicating a first-order relationship with FeOOH surface concentration. A first-order rate expression rather than Monod-type behavior may result from the low FeOOH surface concentration [less than 3 mM in all experiments based on Fe(II) sorption capacity (Figure 7b)]. A previous study found that $Fe(III)_{(aq)}$ bioreduction followed a Monod-type model with a half-saturation constant (K_s) of 29 mM *(15)*. When the initial electron acceptor concentration (FeOOH) is much less than K_s, the Monod rate expression will degenerate into a first-order rate model *(55−57)*. A first-order rate was also observed for the bacterial reduction of a natural Al-goethite by *S. putrefaciens* strain CN32 *(17)*.

The normalized FeOOH reduction rate with respect to lactate concentration followed a Monod-type kinetic relationship (Figure 8b). The initial reduction rate at 30 mM lactate concentration in Figure 8b was averaged from data in Figure 8a (0.027 (±0.0023) h^{-1}). The best-fit Monod rate expression with respect to lactate concentration resulted in a half-saturation constant (K_s) of 0.52 ± 0.1 mM and a maximum reduction rate (V_m) of 0.029 ± 0.002 h^{-1}.

A rate expression for bacterial goethite reduction was formulated as

$$\frac{dC_{goethite}^{total}}{dt} = -S_{goethite}^{free}\frac{V_m C_{lactate}}{K_s + C_{lactate}} \quad (3)$$

where $C_{goethite}^{total}$ is the total FeOOH concentration (M), $S_{goethite}^{free}$ is the surface concentration (M) available for direct organism/DIRB contact, $C_{lactate}$ is the lactate concentration (M), and V_m and K_s are fitted parameters (Figure 8b). Cell growth was not included in eq 3 because the cell concentration of CN32 remains essentially constant during bioreduction experiments when inoculated with high initial cell concentrations (>10^8 cells/mL) *(11)*.

$S_{goethite}^{free}$ is a function of complex properties and phenomena including the total FeOOH concentration; details of the cell-oxide biophysical association; the sorption of Fe(II) and the extent of surface precipitation of $FeCO_3$ on FeOOH; and the surface area, morphology, and aggregation state of the FeOOH particles. It was therefore necessary to make two key assumptions to simulate the experimental bioreduction data (Figures 3 and 4) using rate expression 3: (1) the effective electron acceptor concentration is determined by the concentration variant sorption capacity of Fe(II) on FeOOH (eq 1) and (2) the electron acceptor concentration is reduced by Fe(II) surface complexation and $FeCO_3$ formation on goethite. It was also assumed in the material balance relationship for the electron acceptor that 1 mol of adsorbed Fe(II) or precipitated $FeCO_3$ will reduce 1 mol of the FeOOH surface concentration available for bacterial reduction (e.g., a 1:1 stoichiometric ratio). Assumption 1 allowed direct use of eq 2 to calculate the total goethite surface concentration and to apply eq 3 with determined parameters (K_s and V_m) to express the kinetic rate. Assumption 2 is a simplified approach for modeling the effects of siderite precipitation on goethite bioavailability, which was not well defined by this study. In support of this assumption, the experimental conditions used herein appear optimal for surface assisted nucleation/precipitation as discussed by Stumm et al. *(58)* and Stumm *(59)*. Siderite is relatively slow to precipitate *(60, 61)*, and the circumneutral pH conditions of the bioreduction experiments were optimal for cosorption of Fe(II) *(62)* and CO_3^{2-} *(63)* as requisite for the heterogeneous nucleation of $FeCO_3$. The presence of discrete submicron siderite rhoms in the bioreduced FeOOH (Figure 6), however, indicated that a significant fraction of the biogenic siderite was not associated with goethite as a surface precipitate.

Using these two assumptions, a kinetic model was formulated that coupled the rate expression for microbial activity (eq 3) and the biogeochemical reactions in Table 1. The model involves the following: 7 kinetic equations for total concentrations of lactate, acetate, dissolved CO_2, Fe(II), and goethite (eq 3 and stoichiometric relationship of goethite bioreduction reaction from Table 1), siderite (kinetic expression in Table 1), and total surface site (eq 1 and goethite concentration); 9 equilibrium equations for Fe(II) species: $FeCO_3^0$, $FeHCO_3^-$, $FeOH^+$, $Fe(OH)_2^0$, $Fe(OH)_3^-$, Fe-lactate$^+$, Fe-acetate$^+$, Fe^{2+}-FeOOH, and Fe^{2+}-cell (Table 1); 2 equilibrium equations for HCO_3^- and CO_3^{2-} (pH was fixed at 7); and 4 mass balance equations: total Fe(II), lactate, acetate, and goethite surface sites for the remaining 4 species of Fe^{2+}, lactate$^-$, acetate$^-$, and free goethite surface sites, respectively. These 22 equations were simultaneously solved using a stiff differential-algebraic equation solver (DDASPK) from *(64)*. The combined concentration of Fe(II)-containing aqueous species: Fe^{2+}, $FeCO_3^0$, $FeHCO_3^-$, $FeOH^+$, $Fe(OH)_2^0$, $Fe(OH)_3^-$, Fe-lactate$^+$, and Fe-acetate$^+$ is denoted as $Fe(II)_{(aq)}$ in the simulation of experimental results (Figures 9 and 10). The various simulations (Figures 9 and 10) were generated by adjusting the siderite precipitation rate coefficient (k_f) (Table 1); the best-fit value was 6.0×10^{-6} mM/h, which is close to the value of 5.7×10^{-6} mM/h estimated in *(61)*. Siderite precipitation has been observed at a faster rate (10^{-3}−10^{-5} mM/h) in natural sediments that contain aragonite *(60)*. The experimental data at lower goethite (5 mM) or lactate (0.25 mM) concentrations were well described by the model

TABLE 1. Reactions in the System of Bacterial Reduction of Goethite

reactions	rate
Bacterial Reduction of Goethite	
$4FeOOH + lactate^- + 7H^+ = 4Fe^{2+} + acetate^- + HCO_3^- + 6H_2O$	R^a
Siderite Precipitation	
$Fe^{2+} + CO_3^{2-} = FeCO_3$	$dC_{siderite}/dt = k_f(\{Fe^{2+}\}\{CO_3^{2-}\}/K_{sp} - 1)$
Sorption	
(a) Fe(II) sorption on goethite	
$>$goethite $+ Fe^{2+} = Fe^{2+}$-goethite	equilibrium (eq 2)
(b) Fe(II) sorption on cells	
$>$cell $+ Fe^{2+} = Fe^{2+}$-cell	equilibrium[d]
Equilibrium Aqueous Complex Species	
$Fe^{2+} + CO_3^{2-} = FeCO_3$ (aq)	$\log K = \log(\{FeCO_3\}/(\{Fe^{2+}\}\{CO_3^{2-}\})) = 4.47^b$
$Fe^{2+} + H^+ + CO_3^{2-} = FeHCO_3^+$	$\log K = \log(\{FeHCO_3^+\}/(\{Fe^{2+}\}\{H^+\}\{CO_3^{2-}\})) = 12.32^b$
$Fe^{2+} - H^+ + H_2O = FeOH^+$	$\log K = \log(\{FeOH^+\}\{H^+\}/\{Fe^{2+}\}) = -9.5^b$
$Fe^{2+} + 2H_2O = Fe(OH)_2(aq) + 2H^+$	$\log K = \log(\{Fe(OH)_2\}\{H^+\}^2/\{Fe^{2+}\}) = -20.53^b$
$Fe^{2+} - 3H^+ + 3H_2O = Fe(OH)_3^-$	$\log K = \log(\{Fe(OH)_3^-\}\{H^+\}^3/\{Fe^{2+}\}) = -31^b$
$Fe^{2+} + lactate^- = Fe\text{-}lactate^+$	$\log K = \log(\{Fe - lactate^+\}/(\{Fe^{2+}\}\{lactate^-\})) = -1.82^c$
$Fe^{2+} + acetate^- = Fe\text{-}acetate^+$	$\log K = \log(\{Fe - acetate^+\}/(\{Fe^{2+}\}\{acetate^-\})) = 1.4^b$

[a] Using eq 3 or eq 6. [b] Reference *71*. [c] Reference *1*. [d] Langmuir sorption isotherm, $q = Q\{Fe^{2+}\}/(b + \{Fe^{2+}\})$ with $Q = 4.2 \times 10^{-3}$ mol/10^{12} cells and $b = 5.14 \times 10^{-5}$ M *(15)*.

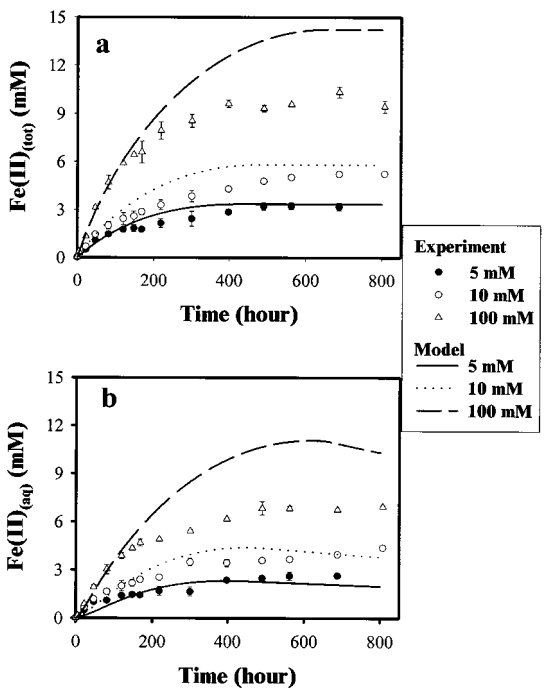

FIGURE 9. Model calculations of goethite reduction by CN32 with variable initial goethite concentrations. The goethite reduction rate was described by eq 3 (text). The siderite precipitation rate and other equilibrium reactions are in Table 1: (a) total Fe(II) and (b) aqueous Fe(II).

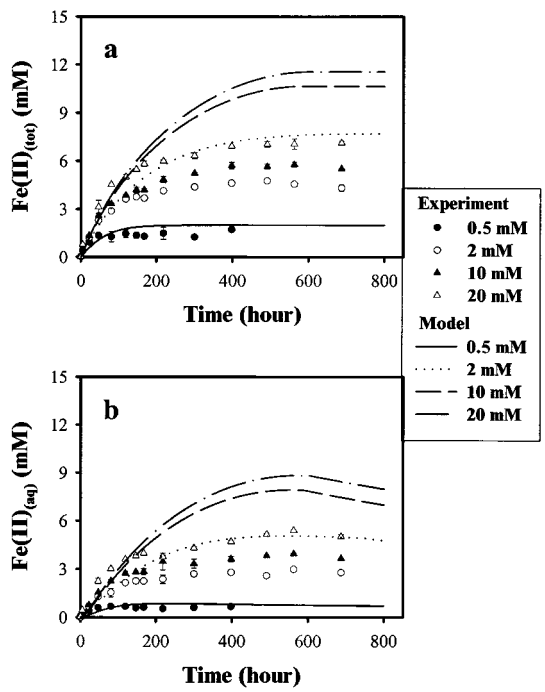

FIGURE 10. Model calculations of goethite reduction by CN32 with variable initial lactate concentrations. The model parameters were the same as in Figure 9.

(Figures 9 and 10). However, the calculations showed increasing disparity as goethite or lactate concentrations were increased.

The disparate model calculations may have resulted from several factors. The aggregation of goethite and the resulting reduction of surface concentration may have been greater than was estimated from eq 2. We have visually observed that CN32 flocculates the FeOOH suspension and through microscopy found that *S. putrefaciens* generates exopolysaccharide that induces interparticle bridging (unpublished results). Also, Fe(II) sorbed to cell surfaces may have affected the reduction rate *(15)*. While we have incorporated this adsorption reaction as a post-reductive sink for biogenic Fe(II) (Table 1), no explicit feedback mechanism was included between biosorption and reduction rate. Biosorbed Fe(II) caused a lag phase and small decrease in the reduction rate of Fe(III)-citrate *(15)*. It is not known whether biosorption in these experiments would promote similar, increased, or decreased effects.

A potentially important factor that was not considered in the above analysis is the Gibbs free energy constraint of electron transfer from lactate to goethite

$$4FeOOH + CH_3CHOHCOO^- + 7H^+ = 4Fe^{2+} + CH_3COO^- + HCO_3^- + 6H_2O$$

$$\Delta G_r = \Delta G_r^0 + 2.3RT\log\left(\frac{\{CH_3COO^-\}\{HCO_3^-\}\{Fe^{2+}\}^4}{\{CH_3CHOHCOO^-\}\{H^+\}^7}\right) \quad (4)$$

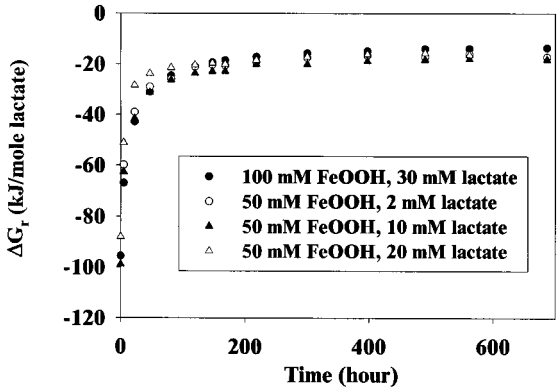

FIGURE 11. Available free energy associated with goethite reduction-lactate oxidation. The reaction free energy was calculated using eq 4 (text), the measured aqueous and total Fe(II) concentrations and reaction stoichiometry (reaction 4).

where $\Delta G_r^o = -222.2$ kJ/mol of lactate (standard formation energy of goethite (−488.7 kJ/mol) is from ref *65* and other species from ref *66*). The residual reaction free energy (ΔG_r) of lactate oxidation to acetate and CO_2 and goethite reduction to Fe(II) at experiment termination for all of the overpredicted cases was approximately about −17.2 (± 1.9) kJ/mol of lactate [based on measured Fe(II) concentrations and the stoichiometric relationship (*4*)] (Figure 11). After correcting for aqueous Fe(II) complexation, the computed ΔG_r value was approximately −22.7 kJ/mol of lactate.

Thermodynamic Analysis. Reaction free energies can affect the rate and extent of abiotic goethite dissolution *(31, 67, 68)*. The macroscopic dissolution of goethite will cease when the free energy of the reaction reaches zero (the equilibrium state) *(31)*. A bacterial reaction, which couple the oxidation of electron donor and reduction of electron acceptor must release enough energy to drive adenosine triphosphate (ATP) synthesis. ATP is synthesized from adenosine diphosphate (ADP) and inorganic phosphate (P_i) through either substrate-level or electron transport phosphorylation *(66)*. The substrate-level phosphorylation is a direct way of making ATP through fermentation of organic compounds (like lactate). ATP synthesis via the electron transport system involves a series of electron transfer and proton release reactions by enzymes and coenzymes associated with the cell membrane and periplasmic space. These reactions result in a proton concentration gradient across the cell membrane with higher proton concentration at periplasm side and higher OH^- in the cytoplasm *(66)*. The chemical potential of this proton gradient is used by ATPase in the membrane to convert adenosine diphosphate (ADP) and inorganic phosphorus (P_i) to ATP (see details in ref *66*). The energy required for ATP production is given by *(1, 66)*

$$\Delta G \pm \Delta G^o + 2.3RT\log\left(\frac{\mathrm{ATP}}{\mathrm{ADPxP_i}}\right) \qquad (5)$$

where ΔG^o is approximately 31.8 kJ/mol ATP *(66)*.

Schink *(69)* analyzed the energetics of ATP synthesis via electron transport phosphorylation in bacterial cells and concluded that −20 kJ/mol was the minimum required for bacteria to exploit the free energy change in a reaction. This value was determined by taking the energy (+50 kJ/mol) required for synthesis of ATP from ADP and P_i under cell conditions (10 mM ATP, 1 mM ADP, and 10 mM P_i) and assuming a heat loss of approximately 20 kJ/mol ATP. Since ATP synthesis from electron transport requires three protons per molecule of ATP, the smallest quantum of energy is approximately −20 kJ/mol or one-third of an ATP unit. This is the amount of energy available to syntrophic partners in methanogen-based degradation processes *(69)* and the value arrived at in our evaluation of the thermodynamic state of goethite-lactate suspension subjected to bioreduction by the dissimilatory Fe(III)-reducing bacterium, *S. putrefaciens* CN32.

Although the reduction of Fe(III) by dissimilatory iron reducing bacterium, *S. putrefaciens* CN32 has been extensively studied, the investigation of biochemistry and energetics of bioreaction coupling lactate oxidation and Fe(III) oxide reduction was limited. However, the fact that Fe(III)/Fe(II) has a very high redox potential ($E^0 = 0.77$ V) and *S. putrefaciens* can use various organic and inorganic electron donors suggests that ATP synthesis for *S. putrefaciens* in the dissimilatory reduction of Fe(III) is mainly through electron transport phosphorylation *(66)*. Direct measurement of respiration-linked proton translocation indicated that the energy generation for *S. putrefaciens* Mr-1 was from electron transport system with either Mn(IV) or Fe(III) as electron acceptor *(70)*. Based on the discussions above and our observation that Fe(III) reduction reaction (eq 4) ceased consistently at about −17.2 kJ/mol (Figure 11) (−22.7 kJ/mol after correcting for Fe(II) complexation), we assumed that the overall reaction of lactate oxidation and goethite reduction must generate more than the defined minimum energy in order to drive ATP synthesis.

Simulation of Bacterial Reduction of Goethite. A general rate law for goethite dissolution that includes a free energy term may be written as *(67, 68)*

$$\frac{\mathrm{d}C_{\mathrm{goethite}}^{\mathrm{total}}}{\mathrm{d}t} = -R_{\mathrm{reduction}}\mathrm{f}(\Delta G_r) \qquad (6)$$

where $R_{\mathrm{reduction}}$ is the rate expression without free energy limit and $\mathrm{f}(\Delta G_r) = 1 - \exp(\Delta G_r/RT)$.

For our case, $R_{\mathrm{reduction}}$ is expressed by eq 3, while $\mathrm{f}(\Delta G_r) = 1 - \exp((\Delta G_r - \Delta G_{\mathrm{min}})/RT)$ (ΔG_r is free energy calculated by eq 4 and ΔG_{min} is the minimum energy required to drive ATP synthesis, R is the gas constant, and T is the absolute temperature). The ΔG_{min} value was −22.7 kJ/mol lactate determined from Figure 11 after correcting for Fe(II) speciation.

Calculation procedures for simulations in Figures 12 and 13 were the same as described before for Figures 9 and 10 except that the rate expression 6 was used here instead of eq 3. Because reaction free energy is a function of reactant and product concentrations, the free energy term in eq 6 has to be updated every iteration and time step. The siderite precipitation rate (k_f) was taken from the previously fitted value of 6×10^{-6} mM/h. The simulated results were in close agreement with the experimental results (Figures 12 and 13), suggesting that the kinetic model was a plausible one for the studied system.

Environmental Implications. This study demonstrated that the rate and extent of goethite reduction by *S. putrefaciens* was a function of electron acceptor and donor concentrations and was constrained by the goethite surface sites availability and overall reaction free energy. The model required several assumptions, including that bacterial reduction of goethite proceeds only when the reaction releases sufficient energy for ATP production and that the reduction rate decreases as the free energy released per unit lactate oxidation decreases. Although the minimum energy of −22.7 kJ/mol lactate was close to those previously reported, independent studies of biochemistry and energetics for *S. putrefaciens* are needed.

Furthermore, the kinetic model was based on the assumption that the goethite surface concentration could be approximated by its sorption capacity for Fe(II). Both Fe(II) sorption and siderite precipitation on goethite may constrain the bioreduction rate by reducing the goethite surface concentration available for bacterial contact/electron trans-

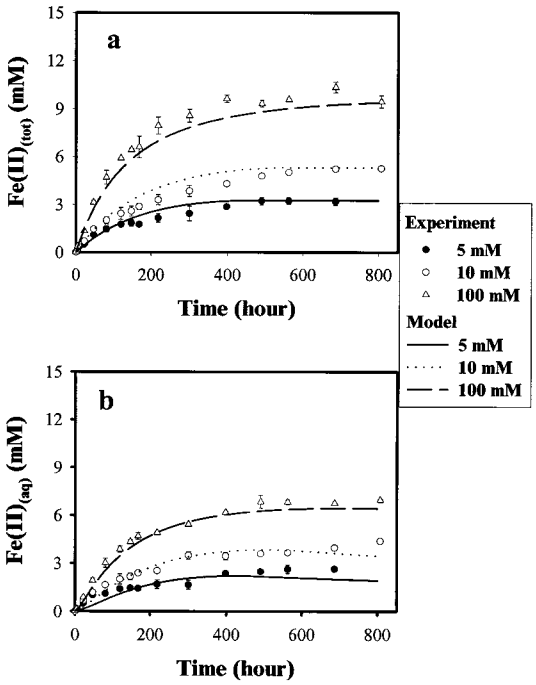

FIGURE 12. Model calculations of goethite reduction by CN32 with variable initial goethite concentrations after the reduction rate was modified with a free energy term eq 6. Other processes are described in Table 1: (a) total Fe(II) and (b) aqueous Fe(II).

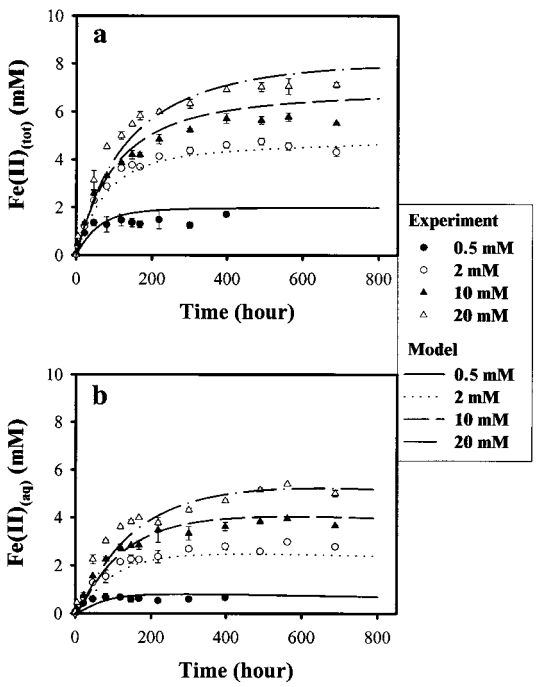

FIGURE 13. Model calculations of goethite reduction by CN32 with variable initial lactate concentrations. Model parameters were the same as in Figure 12.

duction. The assumption that $FeCO_3$ precipitation consumed bioavailable surface sites at 1:1 ratio was not well supported by experimental observation (e.g., significant $FeCO_3$ mass was associated with the interiors of the siderite rhoms). However, we found that the experimental data could not be well simulated with the assumption that Fe(II) sorption was the only biogeochemical reaction to consume surface sites. It is also plausible that bioaggregation of the goethite may have occurred that led to a reduction in site availability.

This investigation and previous studies *(9, 11)* indicate that goethite reduction in batch systems ceases despite excess electron donor. This phenomenon has been attributed to the passivation of the goethite surface by sorbed Fe(II) *(9, 11, 13, 18)*. The observation that advective removal of biogenic Fe(II) can promote goethite reduction *(10, 14)* supports the surface passivation hypothesis. This study, however, indicates that siderite precipitation on goethite and free energy constraints may also limit the bioreduction of crystalline Fe(III) oxides. The modeling study highlights the potential importance of free energy as a biodissolution constraint because the apparent effects of Fe(II) sorption and siderite precipitation, alone, were insufficient to account for the decreased reduction of goethite at both higher goethite and lactate concentrations. The observed increases in goethite reduction that accompany advective removal of Fe(II) *(10, 14)* or Fe(II) aqueous complexation *(18)* may result from a combination of factors including decreased Fe(II) sorption and $FeCO_3$ precipitation and relaxation of the free energy constraint.

Acknowledgments

This research was supported by the U.S. Department of Energy (DOE), Office of Basic Energy Science (BES), Engineering and Geosciences Division, under contract DE AC06-76 RLO 1830. Pacific Northwest National Laboratory is operated for the DOE by Battelle Memorial Institute. We thank four anonymous reviewers for their valuable comments and suggestions.

Literature Cited

(1) Arnold, R. G.; Olson, T. M.; Hoffmann, M. R. *Biotechnol. Bioeng.* **1986**, *28*, 1657−1671.
(2) Tugel, J. B.; Hines, M. E.; Jones, G. E. *Appl. Environ. Microbiol.* **1986**, *52*, 1167−1172.
(3) Caccavo, F. J.; Blakemore, R. P.; Lovley, D. R. *Appl. Environ. Microbiol.* **1992**, *58*, 3211−3216.
(4) Lovley, D. R. *Microbiol. Rev.* **1991**, *55*, 259−287.
(5) Lovley, D. R.; Philips, E. J. P. *Appl. Environ. Microbiol.* **1986**, *52*, 752−757.
(6) Arnold, R. G.; DiChristina, T. J.; Hoffmann, M. R. *Biotechnol. Bioeng.* **1988**, *32*, 1081−1096.
(7) Fisher, F. G.; Pfanneberg, T. *Zentralbl Mikrobiol* **1984**, *139*, 163−166.
(8) Lovley, D. R.; Philips, E. J. P. *Appl. Environ. Microbiol.* **1987**, *523*, 1536−1540.
(9) Roden, E. E.; Zachara, J. M. *Environ. Sci. Technol.* **1996**, *30*, 1618−1628.
(10) Roden, E. E.; Urrutia, M. M. *Environ. Sci. Technol.* **1999**, *33*, 1847−1853.
(11) Zachara, J. M.; Fredrickson, J. K.; Li, S.-M.; Kennedy, D. W.; Smith, S. C. *Am. Mineralogist* **1998**, *83*, 1426−1443.
(12) Fredrickson, J. K.; Zachara, J. M.; Kennedy, D. V.; Dong, H.; Onstott, T. C.; Hinman, N. W.; Li, S.-m. *Geochim. Cosmochim. Acta* **1998**, *62*, 3239−3257.
(13) Urrutia, M. N.; Roden, E. E.; Fredrickson, J. K.; Zachara, J. M. *Geomicrobiology* **1998**, *15*, 269−291.
(14) Roden, E. E.; Urrutia, M. M.; Mann, C. J. *Appl. Environ. Microbiol.* **2000**, *66*, 1062−1065.
(15) Liu, C.; Zachara, J. M.; Gorby, Y. A.; Szecsody, J. E.; Brown, C. F. *Environ. Sci. Technol.* **2001**, *35*, 1385−1393.
(16) Lovley, D. R.; Coates, J. D.; Blunt-Harris, E. L.; Phillips, E. J. P.; Woodward, J. C. *Nature* **1996**, *382*, 445−448.
(17) Kukkadapu, R. K.; Zachara, J. M.; Smith, S. C.; Fredrickson, J. K.; Liu, C. *Geochem. Cosmochim. Acta* **2001**, in press.
(18) Urrutia, M. N.; Roden, E. E.; Zachara, J. M. *Environ. Sci. Technol.* **1999**, *33*, 269−291.
(19) Rittmann, B. E.; VanBriesen, J. M. *Rev. Mineralogy* **1996**, *34*, 311.
(20) Salvage, K. M.; Yeh, G. T.; Cheng, H. P.; Cheng, J. R. Development of a model of subsurface hydrologic transport and biogeochemical reactions (HYDROBIOGEOCHEM). In *Computational Methods in Water Resources XI*; 1996.
(21) Van Cappellen, P.; Gaillard, J. F.; Rabouille, C. Biogeochemical transformations in sediments: Kinetic models of early diagenesis. In *Interactions of C, N, P, and S biogeochemical cycles and*

global change; Wollast, R., Mackenzie, F. T., Chou, L., Eds.; Springer: Berlin, 1993; pp 401−445.
(22) McNab, W. W.; Narasimhan, T. N. *Water Resources Res.* **1994**, *30*, 2619−2635.
(23) Tebes-Stevens, C.; Valocchi, A. J.; VanBriesen, J. M.; Rittmann, B. E. *J. Hydrology* **1998**, *209*, 8−26.
(24) Chilakapati, A.; Ginn, T.; Szecsody, J. E. *Water Resources Res.* **1998**, *34*, 1767−1780.
(25) Wood, B. D.; Dawson, C. N.; Szecsody, J. E.; Streile, G. P. *Water Resources Res.* **1994**, *30*, 1833−1845.
(26) Yeh, G. T.; Tripathi, V. S. *Water Resources Res.* **1991**, *27*, 3075−3094.
(27) Viswanathan, H. S.; Robinson, B. A.; Valocchi, A. J.; Triay, I. R. *J. Hydrology* **1998**, *209*, 251−280.
(28) Essaid, H. I.; Bekins, B. A.; Godsy, E. M.; Warren, E. *Water Resources Res.* **1995**, *31*, 3309−3327.
(29) Clement, T. P.; Sun, Y.; Hooker, B. S.; Petersen, J. N. *Ground Water Monitoring Remediation* **1998**, *Spring*, 79−92.
(30) Steefel, C. I.; Van Cappellen, P. *J. Hydrology* **1998**, *209*, 1−7.
(31) Kraemer, S. M.; Hering, J. G. *Geochem. Cosmochim. Acta* **1997**, *61*, 2855−2866.
(32) Schwertmann, U.; Cornell, R. M. *Fe Oxides in the Laboratory: Preparation and Characterization*; VCH Publishers: Weinheim, Germany, 1991.
(33) Liu, Y.; Fredrickson, J. K.; Gorby, Y. A.; Wildung, R. G.; Balkwill, D. L.; Ringelberg, D.; Taylor, W. H.; Boone, D. R. *Appl. Environ. Microbiol.* **2000**, submitted.
(34) Balch, W. E.; Fox, G. E.; Magrum, L. J.; Woese, C. R.; Wolfe, R. S. *Microbiol. Rev.* **1979**, *43*, 260−296.
(35) Monod, J. *Annual Rev. Microbiol.* **1949**, *3*, 371−393.
(36) Gaudy, A. F. J.; Gaudy, E. T. *Microbiology for environmental scientists and engineers*; McGraw-Hill: 1980.
(37) Benoit, G.; Oktay-Marshall, S. D.; Cantu, A.; Hood, E. M.; Coleman, C. H.; Corapcioglu, M. O.; Santschi, P. H. *Marine Chem.* **1994**, *45*, 307−336.
(38) Sanudo-Wilhelmy, S. A.; Rivera-Duarte, I.; Flegal, A. R. *Geochem. Cosmochem. Acta* **1996**, *60*, 4933−4944.
(39) Stordal, M. C.; Gill, G. A.; Wen, L.-S.; Santschi, P. H. *Limnol. Oceanogr.* **1996**, *41*, 52−61.
(40) Benoit, G. *Geochem. Cosmochem. Acta* **1995**, *59*, 2677−2687.
(41) Balistrieri, L. S.; Murray, J. W.; Paul, B. *Geochem. Cosmochem. Acta* **1994**, *58*, 3993−4008.
(42) Li, Y.-H.; Burkhardt, L.; Buccholtz, M.; O'Hara, P.; Santschi, P. H. *Geochemica et Cosmochemica Acta* **1984**, *48*, 2011−2019.
(43) Honeyman, B. D.; Santschi, P. H. *Environ. Sci. Technol.* **1988**, *22*, 862−871.
(44) Pan, G.; Liss, P. S.; Krom, M. D. *Colloids Surfaces* **1999**, *151*, 127−133.
(45) Morel, F. M. M.; Gschwend, P. M. The role of colloids in the partitioning of solutes in natural waters. In *Aquatic Surface Chemistry*; Stumm, W., Ed.; Wiley: 1987; pp 405−422.
(46) Honeyman, B. D.; Santschi, P. H. *J. Mar. Res.* **1989**, *47*, 951−992.
(47) DiToro, D. M.; Mahony, J. D.; Kirchgraber, P. R.; O'Byrne, A. L.; Pasquale, L. R.; Piccirilli, D. C. *Environ. Sci. Technol.* **1986**, *20*, 55−61.
(48) Chang, C. C. Y.; Davis, J. A.; Kuwabara, J. S. *Estuarine, Coastal Shelf Sci.* **1987**, *24*, 419−424.
(49) Anderson, M. A.; Tejedor-Tejedor, M. I.; Standorth, R. R. *Environ. Sci. Technol.* **1985**, *19*, 632−637.
(50) Lovley, D. R.; Philips, E. J. P. *Appl. Environ. Microbiol.* **1988**, *54*, 1472−1480.
(51) Sposito, G. *The Thermodynamics of Soil Solutions*; Oxford University Press: 1981.
(52) Cornell, R. M.; Schwertmann, U. *The Iron Oxides*; VCH: Weinheim, Germany, 1996.
(53) Davis, J. A.; Kent, D. B. Surface complexing modeling in aqueous geochemistry. In *Mineral-Water Interface Geochemistry*; White, M. F. H. a. A. F., Ed.; Mineral. Soc. America: 1990; Vol. 23, pp 177−260.
(54) Zachara, J. M.; Fredrickson, J. K.; Smith, S. C. *Geochim. Cosmochim. Acta* **2000**, *Accepted*.
(55) Liu, C.; Zachara, J. M. *Environm. Sci. Technol.* **2001**, *35*, 133−141.
(56) Robinson, J. A. *Adv. Microbial Ecology* **1985**, *8*, 61−114.
(57) Simkins, S.; Alexander, M. *Appl. Environ. Microbiol.* **1984**, *1984*, 1299−1306.
(58) Stumm, W.; Furrer, F.; Kunz, B. *Croat. Chem. Acta* **1983**, *56*, 593−611.
(59) Stumm, W. *Chemistry of the Solid-Water Interface*; John Wiley & Sons: 1992.
(60) Wajon, J. E.; Ho, G.-E.; Murphy, P. J. *Water Res.* **1985**, *19*, 831−837.
(61) Hunter, K. S.; Wang, Y.; Van Cappellen, P. *J. Hydrology* **1998**, *209*, 53−80.
(62) Zachara, J. M.; Smith, S. C.; Fredrickson, J. K. *Geochim. Cosmochim. Acta* **2000**, *64*, 1345−1362.
(63) van Geen, A.; Robertson, A. P.; Leckie, J. O. *Geochim. Cosmochim. Acta* **1994**, *58*, 2073−2086.
(64) Brown, P. N.; Hindmarsh, A. C.; Petzold, L. R. *SIAM J. Sci. Comput.* **1998**, *19*, 1495−1512.
(65) Robie, R. A.; Hemingway, B. S.; Fisher, J. R. Thermodynamics properties of minerals and related substances at 248.15 K and 1 bar pressure and at higher temperatures. In *U.S. Geol. Surv. Bull.*; 1978.
(66) Brock, T. D.; Madigan, M. T.; Martinko, J. M.; Parker, J. *Biology of Microorganisms*, 7th ed.; Prentice-Hall: Englewood Cliff, NJ, 1994.
(67) Lasaga, A. C. Transition state theory. In *Kinetics of Geochemical Processes*; Lasaga, A. C., Ed., 1981; Vol. 8, pp 135−169.
(68) Aagaard, P.; Helgeson, H. C. *Am. J. Sci.* **1982**, *282*, 237−285.
(69) Schink, B. *Microbiol. Molecular Biol. Rev.* **1997**, *61*, 262−280.
(70) Myers, C. R.; Nealson, K. H. *J. Bacteriol.* **1990**, *172*, 6232−6238.
(71) Allison, J. D.; Brown, D. S.; Novo-Gradac, K. J. *MINITEQA2// PRODEFA2, A geochemical assessment model for environmental systems (version 3)*; Environmental Research Laboratory, USEPA: 1991.

Received for review December 11, 2000. Revised manuscript received March 22, 2001. Accepted March 27, 2001.

ES001956C